Tribology International 192 (2024) 109307

Contents lists available at ScienceDirect

Tribology International

journal homepage: www.elsevier.com/locate/triboint

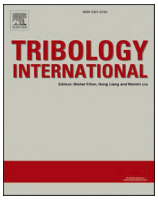

Friction control by load-induced structure modification of overbased detergent in fully formulated lubricant

Y. Guan [a,*], E. Marquis [c], M. Clelia Righi [c], J. Galipaud [a], F. Dubreuil [a], J. Dufils [b], E. Macron [b], F. Dassenoy [a], M.-I. de Barros Bouchet [a,*]

[a] University of Lyon, Ecole Centrale de Lyon, Laboratory of Tribology and System Dynamics, CNRS UMR5513, Ecully, France
[b] HEF/IREIS, Avenue Benoît Fourneyron, Andrézieux-Bouthéon, France
[c] Department of Physics and Astronomy, University of Bologna, Bologna 40127, Italy

ARTICLE INFO

Keywords:
A-C:H DLC
Fully formulated lubricant
Overbased detergent
Calcium carbonate polymorphs

ABSTRACT

The increasing application of diamond-like carbon (DLC) coatings in engine mechanical parts requires the investigation on interaction mechanism between DLC and fully formulated engine oil. This study shows that the friction can be controlled by monitoring the load for a steel/DLC contact, lubricated by a fully formulated 5W30 engine oil in boundary/mixed lubrication regime. A calcium carbonate-rich patchy tribofilm, mainly formed on steel ring, was characterized by multiple surface analyses. X-ray photoelectron spectroscopy (XPS) indicates an increase quantity of calcium carbonate ($CaCO_3$) with increasing contact load. Transmission Electron Microscope (TEM) showed that the original calcium carbonate in the overbased detergent additive within the lubricant itself was amorphous. However, the amorphous calcium carbonate crystallizes in vaterite (low load), aragonite (medium load) and calcite (high load) during the tribological tests. The intrinsic lubricity of each calcium carbonate polymorph was estimated by density functional theory calculations, while the tribological properties of the sliding interface composed by H-passivated diamond and $CaCO_3$ polymorphs were investigated by ab initio molecular dynamic simulations. The in-depth investigation presented here sheds light into the main factors leading to the unexpected pressure-induced friction reduction.

1. Introduction

The friction reduction in the automobile industry is not only a concern of fuel economy but also an environmental issue. Diamond-Like Carbon (DLC) has been increasingly used as solid lubricant coating to protect coating on mechanical parts in internal combustion engines, thanks to its excellent wear resistance [1] and superlubricity [2–4] under boundary/mixed lubrication regimes.

Most of the studies on the interaction mechanism between DLC coatings and engine oils have been conducted by using base oil blending with one or two additives, for example, molybdenum dithiocarbamate (MoDTC) and zinc dialkyldithiophosphate (ZDDP). De Barros Bouchet et al. [5] investigated the interaction of these traditional additives with hydrogenated and hydrogen-free DLC coatings. A better affinity of these additives was found when hydrogenated DLC is involved in tribo-pair. Spikes's [6] group compared the tribological behaviors in boundary lubrication regime, of five different DLC coatings with different dopants and hydrogen contents, in the presence of base oil mixed with ZDDP. The results indicate that ta-C DLC provides lowest friction but the highest wear, while a relatively low wear was observed for a-C:H and a-C DLC coatings. Kalin and his coworkers [7] investigated the thickness and the composition of ZDDP tribofilm with mixed and self-mated contact of DLC-steel. The formation of the tribofilm was observed on both surfaces although its thickness was lower on the DLC than on the steel surfaces. However, one of the limitations of these researches is that the results may not be able to meet the practical requirements due to the improper selected lubricants.

Several studies were realized by using commercial engine oils. For example, Neville and her group [8] selected a-C:H DLC to perform ball-on-disk friction tests in boundary lubrication regime with two types of fully formulated oils: one containing a ZDDP and a calcium detergent, the second one composed of sulfur-based extreme pressure (EP) additive and antioxidant. For both oils, the a-C:H DLC/steel tribo-pair always provides the lowest friction. They also point out the lower tribo-chemical reactivity of hydrogenated DLC with sulfur-based EP additive. However, the detailed interpretation of low friction was not

* Corresponding authors.
E-mail addresses: yue.guan@ec-lyon.fr (Y. Guan), maria-isabel.de-barros@ec-lyon.fr (M.-I. de Barros Bouchet).

https://doi.org/10.1016/j.triboint.2024.109307
Received 1 November 2023; Received in revised form 23 December 2023; Accepted 15 January 2024
Available online 19 January 2024

given. Similarly, in another study of Neville [9], the tribological performances of fully formulated lubricant with and without organic friction modifier for a-C:H DLC/steel mixed contact was investigated. Although the role of other lubricant additives, such as calcium-based detergent and nitrogen-based dispersants was mentioned, no further related investigations have been performed. However, these additives could play some irreplaceable roles during the friction.

Detergent additives are crucial in the formulation of lubricants for automobiles. They can serve several essential purposes, such as neutralizing acidic combustion by-products to minimize corrosive wear, neutralizing acidic lubricant oxidation products, and acting as a "detergent" to prevent the buildup of deposits on high-temperature surfaces like pistons. The chemical composition of detergent additives consists of two primary components [10]: a metal surfactant salt and an inorganic base stabilized by this surfactant. The inorganic bases are generally in form of calcium or magnesium carbonate. The detergent that contains a core of inorganic bases is called overbased detergent, otherwise, neutral detergent. The impacts of detergent additives on the tribological behaviors of steel contacts have been widely explored [11–17]. For example, T. Costello et al. [12] performed the four ball tests with the lubricant containing overbased sulfonates and sulfurized olefins. The results given by X-ray absorption near edge structure (XANES) spectroscopy showed that the presence of sulfurized olefins can improve the extreme pressure performance of the lubricant by the formation of $CaSO_4$ and FeS. In another study, the group of H. Spikes [13] compared the tribological behaviors of four different overbased calcium sulphonate detergents. Two of the four detergents gave relatively low boundary friction coefficients, while the other two showed considerably higher boundary friction. These differences were attributed to the different alkyl chain structures of the detergent additives. Nevertheless, very few studies are reported on their effect on DLC coatings.

In this study, the effect of contact pressure on the friction response of a commercial fully formulated lubricant including a detergent additive was investigated in presence of a steel/DLC contact in boundary/mixed lubrication regime. After the friction tests, optical microscope, interferometer and Scanning Electron Microscope (SEM) equipped with Energy Dispersive X-ray Spectroscopy (EDS) were used to characterize the topography and the surface chemical composition of the rubbed surface. X-ray photoelectron spectroscopy (XPS) provided the quantification of the elements constitute the tribofilm as well as their chemical states. Focused Ion Beam (FIB) nanomachining was used for the transversal cut preparation conducted to prepare the foils on tribofilm for Transmission Electron Microscope (TEM) characterization. Fourier Transform Infra-Red (FTIR) spectroscopy was also employed to further analyze the chemical bonds on surface. Finally, numerical simulations within the density functional theory (DFT) are also presented to investigate the fundamental tribological behavior of tribofilm ruling at the nanoscale.

2. Experimental section

2.1. Materials

A hydrogenated a-C:H DLC was prepared by HEF IREIS company. An intermediate layer was applied onto the steel surface to improve the adhesion of the DLC films. The mirror-polished M2 steel disks were coated with 2 micrometers of DLC. Their mechanical properties are characterized by nano-intendation [18], the results are reported in Table 1.

Table 1
The mechanical properties of M2 steel and a-C:H DLC coating.

Name	Composition	Hardness	Elastic modulus
M2 steel	0.85% C, 6% W, 5% Mo, 4% Cr, 2% V	64 HRC	210 GPa
100Cr6 steel	0.95% C, 0.25% Mn, 0.15% Si, 1.5% Cr	223 HB	210 GPa
a-C:H DLC	20% H, 80% C	27 GPa	259 GPa

The 100Cr6 steel ring has a diameter of 35 mm and a shoulder of 8 mm leading to a 8 mm long line contact when the ring is rubbed against the disk. The root mean square surface roughness (Sq) before and after the friction tests was measured by an optical white light interferometer (Contour GT-K1, Bruker) at scale of 230 μm * 180 μm in at least 3 areas. Before the sliding tests, the Sq values for steel ring and a-C:H DLC are 240 nm ± 20 nm and 8 nm ± 1 nm, respectively. One representative measurement was given for each sample in Figure. S1. The lubricant used in this study was a commercial fully formulated ELF SXR 900 5W30 engine oil (Totalenergies, France) with the kinematic viscosity of 9.3 cSt at 100 °C, TBN value of 10mgKOH/g. XPS was performed on this lubricant in order to have a basic recognition on its composition. The detailed procedures and obtained XPS survey spectrum are shown in Fig. S2. Based on XPS analysis, it appears that ZDDP-like antiwear additive and calcium carbonate overbased detergent additive were contained in lubricant. No molybdenum-based friction modifier (as MoDTC, etc.) was detected.

2.2. Friction experiments

Ring-on-disk sliding tests were performed in company HEF IREIS by using a homemade reciprocating tribometer. A detailed description of tribometer is shown in Figure. S3. Fig. 1 shows a schematic of the tribo-pair. The tribo-system made of a steel ring and a a-C:H DLC disk was immersed in a lubricant bath. The tests were performed at 100 °C, a-C:H DLC moved reciprocally with an average speed of 0.001 m/s, 3 mm stroke length, in order to keep constant contact pressure even if the wear occurs. The normal load was applied on the a-C:H DLC disk. Three loads of 400 N, 950 N and 2100 N were used for the tribological tests, corresponding to the maximum Hertzian contact pressures of 320 MPa, 500 MPa and 740 MPa respectively. The rotation speeds of the steel ring during the test were 2.66 m/s, 2.38 m/s, 2.16 m/s, 1.83 m/s, 1.56 m/s, 1.43 m/s, 1.21 m/s, 1.01 m/s, 0.82 m/s, 0.64 m/s. At each rotation speed, the steady state coefficient of friction (CoF) was recorded and the tests were repeated 3 times. The total test duration was 40 min. The alignment is enabled by the disk sample holder which was designed by HEF IREIS company in order to facilitate ring/disk alignment. Due to the relatively thin DLC coatings (2 μm), the overall contact pressure at a macroscopic level was primarily influenced by the mechanical properties of the steel substrate. In this test configuration, the lubrication regime corresponds to boundary lubrication at low rotation speed of steel ring, and mixed lubrication at high rotation speeds of steel ring. The calculation of the lubrication regimes follows the formula for line contact in reference 19 and 20.

2.3. Surface analysis, microscopy and topography

After each friction test, the steel rings and the a-C:H DLC disks underwent two rounds of cleaning in an ultrasonic bath filled with n-heptane (Chimie Plus laboratoires, content > 99%) for a duration of 10 min each. This process was essential to eliminate any remaining traces of oil. The wear conditions on rings and disks were measured by Taylor Hobson profilometer (PGI 820). The wear tracks were observed without any conductive coating, by using SEM (FEI XL30-FEG) equipped with an Everhardt-Thornley secondary electron detector. The observations were conducted under high vacuum conditions (10^{-6}mbar). The acceleration voltage was set at 20 kV for steel materials, while 9 kV for a-C:H DLC. Chemical composition analyses were carried out by EDX using an Oxford Instruments X-max silicon drift detector. Quantitative analysis of the EDX spectra was performed using the Aztec software.

Extreme surface analysis was conducted by XPS on both rings and disks using an ULVAC-PHI Versa Probe III spectrometer equipped with a monochromatic Al Kα X-ray source, with a beam diameter of 200 μm. The binding energy scale was calibrated based on the C1s photo-peak at

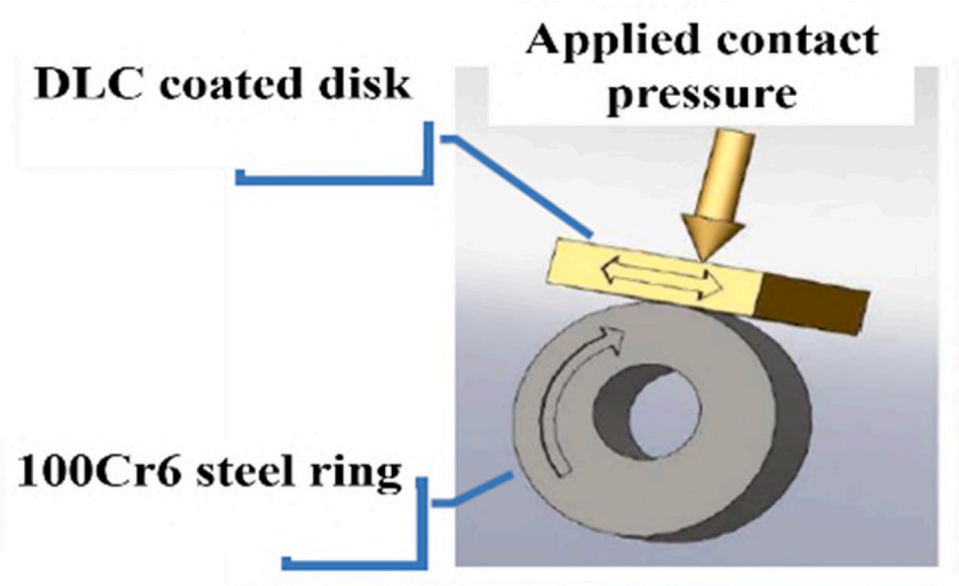

Fig. 1. The schematic of ring-on-disk configuration.

a binding energy of 284.8 eV, with an estimated error of ± 0.1 eV. Initially, a survey spectrum was obtained using a pass energy of 224 eV, to identify all the elements present on the surface. Subsequently, high resolution spectra were recorded with a range of 20 eV using a pass energy of 13 eV. These scans aimed to accurately determine the chemical state of each element and carry out quantitative analysis utilizing PHI Multipack software. To account for the background contribution, the Shirley method was employed, and Wagner sensitivity factors (adjusted for the transmission function of the instrument) were utilized to calculate the atomic concentrations.

Dual Beam Focused Ion preparation was employed to prepare thin cross-sections of the wear track on both steel rings and a-C:H DLC disks by Manutech-USD (Saint-Etienne, France). To protect the surfaces during milling and prevent re-deposition, a platinum gaseous precursor was initially used to deposit a platinum layer onto the samples' surface. This deposition process occurred in two stages. Firstly, a low-energy electron beam was employed to prevent any damage to the samples' surface. Subsequently, a high-energy Ga ion beam was employed to enhance the growth rate of the protective platinum film and expedite the process. The resulting thin FIB cuts were then observed using a Jeol 2100 F-UHR TEM, equipped with a Schottky field emission gun. Bright-Field (BF) images were captured using a Gatan Orius 100 CCD camera, while Dark-Field (DF) images were acquired in the Scanning Transmission Electron Microscopy (STEM) mode. For local chemical analysis (spectra or elemental maps), EDS (80 mm^2 silicon drift detector from Oxford Instruments) was employed. A FIB cut preparation made from the 740 MPa steel ring was also observed and analyzed by using FEI Titan ETEM G2 electron microscope operating at 300 keV and equipped with a Cs image aberration corrector.

FTIR analysis was carried out on steel rings at 320 MPa, 500 MPa and 740 MPa using a JASCO FT/IR-6600 spectrometer. The resolution was 4.0 cm^{-1} with a corresponding aperture diameter of 7.1 mm. The data was exported by software SpectraManager™.

3. Simulation

We performed Density Functional Theory (DFT) calculations by means of the 6.7 version of the Quantum ESPRESSO package [21]. For the Ab Initio Molecular Dynamics (AIMD) simulations of sliding surfaces, we used a version of the code modified by our group. The generalized gradient approximation (GGA) within the Perdew–Burke–Ernzerhof (PBE) was used to describe the electronic exchange–correlation [22]. The electronic wave-functions were expanded on a plane-waves basis truncated with a cutoff of 35 Ry, while a cutoff of 280 Ry was used for the charge density. The ionic species were described by ultrasoft pseudopotentials, and we adopted default criteria for energy and forces convergence. To describe the occupation of the electronic states we employed a Gaussian smearing of 0.02.

To model calcium carbonate surfaces, we started from the bulk structures of calcite, aragonite and vaterite. For each of the $CaCO_3$ polymorphs we built the most stable surface among those with a neutral overall charge, i.e., calcite (104), aragonite (011) and vaterite (010) [23,24]. The thickness of each slab has been set to $(CaCO_3)_8$ units, then at least 15 Å of vacuum was added on the z direction to avoid lateral interactions between replicas. To model the a-C:H DLC surface, we employed a fully H-passivated (111) diamond facet, already optimized as described in a previous work [25]. During relaxations, the Brillouin zone was sampled with a 2 × 1 × 1 Monkhorst-Pack grid, ensuring the convergence of the K-points sampling on the total energy. For the AIMD simulations, only the Γ point has been sampled, since 2 × 1 supercells were employed. $CaCO_3$ @$CaCO_3$ interfaces were built starting from the relaxed surfaces, by reflecting along the z axis, for each of the three calcium carbonate polymorphs. Although the use of supercells, for the heterogeneous $CaCO_3$ @diamond interfaces, a small mismatch between the lattice parameters of each CaCO3 polymorph and the diamond was inevitably introduced. However, variable-cell relaxations were performed to minimize the residual stress acting laterally on the xy plane. The adhesion energy between surfaces was evaluated for both homogenous and heterogeneous interfaces. The work of separation (W_{SEP}) is then calculated with the following formula:

$$W_{SEP} = \frac{E_{S1} + E_{S2} - E_{S1+S2}}{A_{cell}},$$

Where E_{S1} and E_{S2} are the total energies of the isolated surfaces, E_{S1+S2} is the total energy of the interface, and Acell is the area of the supercell. The work of separation was evaluated at different lateral positions (x,y), in order to identify the most favorite coupling, i.e., the (x,y) lateral position leading to the higher binding energy between surfaces. The potential corrugation (ΔW_{SEP}), defined as the difference between the maximum and minimum values of WSEP encountered when exploring all possible lateral couplings, has been evaluated for homogeneous $CaCO_3$ interfaces. Relaxations of the minimum- and maximum- energy configuration were repeated in the presence of an external load of 1, 2, 5

and 8 GPa, applied perpendicularly to the interfaces.

AIMD simulations of about 20 picoseconds duration were carried out for three $CaCO_3$ @diamond hetero-interfaces. Newton's equations of motion were integrated using the Verlet algorithm. The time step, Δt was chosen in order to sample at least 10 times the highest bond-vibration frequency. For heterogeneous $CaCO_3$ @diamond interfaces we used a timestep of 1.45 fs, due to the presence of low-weight atoms (H, with the mass of deuterium. The temperature was kept constant at 300 K during the AIMD simulations, by separately rescaling the velocities of the two surfaces.

4. Results

4.1. Tribological results

The friction coefficient as function of the ring rotation speed at 320 MPa, 500 MPa and 740 MPa is shown in Fig. 2. The good repeatability is confirmed by the friction curves shown in Figure. S4. The black spots, red spots and blue spots correspond to the contact pressure of 320 MPa, 500 MPa and 740 MPa, respectively. The CoF decreases as the function of the rotation speed of the steel ring and the contact pressure.

According to the Stribeck curve, in boundary/mixed lubrication regime, the CoF should increase as the test conditions become more severe. In consequence, as the rotation speed increases, a lower CoF is expected, while as the contact pressure increases, a higher CoF is expected. Conversely, we obtained a reduction of the CoF with the increasing of pressure, independently on the rotation speed of the steel ring. The Sq values of the steel ring and the a-C:H DLC after the friction tests were 240 nm ± 20 nm and 10 nm ± 1 nm (Figure. S2). The initial Sq values on steel ring and a-C:H DLC disk are 260 nm ± 20 nm and 9 nm ± 1 nm. Therefore, it is unlikely that the friction reduction was simply driven by a self-polishing effect.

The optical images recorded on the virgin a-C:H DLC disk and the virgin steel ring are shown in Fig. 3 (a1) and (b1), respectively. The wear tracks on the a-C:H DLC disks and the steel rings after the friction tests are shown in Fig. 3 (a2 – a4) and (b2 – b4), respectively. The 3 mm wear width on a-C:H disks is corresponding to the stroke length. The wear length is about 8 mm (not shown in the image) is corresponding to the line contact length.

Comparing with virgin a-C:H DLC surfaces, a1 (no friction), it can be noticed the absence of visible tribofilm on the a-C:H DLC surfaces after the friction tests. This indicates either the presence of a super thin tribofilm, not optically visible, or that only few chemical interactions occur between the a-C:H DLC and the lubricant. In contrary, comparing Fig. 3 b1 with b2, b3 and b4, the presence of a tribofilm on the steel ring was detected although the high surface roughness. The wear measurements on the a-C:H DLC disks are given in Figure. S5. The wear depth on the a-C:H DLC fluctuates between 30 nm to 50 nm, and did not appear to be closely related to the contact pressure. For the steel ring, the wear depth and wear volume were not identified by interferometer or profilometer due to the high surface roughness. The wear can be further confirmed by FIB cut preparation, which will be introduced in the following text.

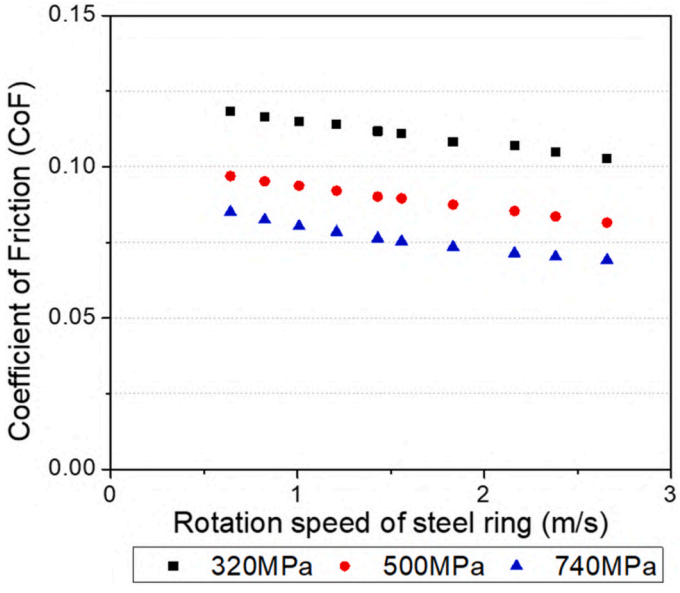

Fig. 2. Friction curves at 320 MPa (black dots), 500 MPa (red dots) and 740 MPa (blue dots).

4.2. Surface analyses and TEM characterizations of tribofilm

X-ray Photoelectron Spectroscopy (XPS) was used to analyze inside and outside the wear tracks on topmost 10 nm of the a-C:H DLC disks and steel rings, with the objective to investigate the chemical composition of the rubbed surfaces. The binding energies (BEs) of photo-peaks: C1s, O1s, P2p, S2p, Ca2p3/2, Fe2p3/2, and Zn2p3/2 were examined. The quantification of each element was also conducted. It can be seen that the oxidation states of the various elements (P, S, Zn, Ca, Fe, C, O) are fairly similar after the friction tests at the three contact pressures for both surfaces (as shown in Figure. S6).

The quantification results on a-C:H disks and steel rings, are listed in Table 2. On the a-C:H disk, P, S, Ca and Zn displayed a very low concentration and a tendency to decrease as the function of the pressure. The low content of these elements is consistent with the optical images (Fig. 3 a2 - a4) where the tribofilm could hardly be observed. On the counterpart, the concentration of P, S, Ca and Zn was found to be higher. The quantity of some elements such as S and Zn also tended to decrease with the pressure, while the concentration of P slightly increases. Interestingly, among the characteristic elements (P, S, Ca and Zn), a significant increase of the Ca element was observed in a ratio of almost 80% at 740 MPa, comparing with 320 MPa. The presence of calcium can be tracked back to the original composition of the detergent additive, in which it is normally found in the form of calcium carbonate. The quantity variation of C and O is hard to be discussed due to the fact that they can de derived from various sources, such as surface contamination, alkyl groups from lubricants, etc.

Fig. 4 shows the fitting results for C1s (a) and Ca2p (b) high resolution photo-peaks on steel ring at 320 MPa, 500 MPa and 740 MPa. Ca2p doublet was fitted by a binding energy difference set at 3.60 eV. The area ratio was set at Ca2p3/2 (dark green): Ca2p1/2 (light green) = 2: 1. For the C 1 s peak, the blue, red, yellow and green contributions correspond to the C-C/C-H (284.8 eV), C-O (286.2 eV), C═O (288.1 eV) and CO_3 (289.9 eV), respectively. On the other hand, the contribution of Ca2p3/2 located at 347.5 eV is found to correspond to calcium carbonate. Full-width-half-maximum (FWHM, identical for all C1s contributions) and detailed binding energy measured of each for the three pressures were given in Table 3.

To have a deeper understanding of the calcium carbonate structure, TEM-FIB was carried out on the tribofilm obtained on the steel rings. First of all, SEM/EDS was used to localize a position rich in calcium element. Fig. 5 shows the secondary electron images of steel rings at 320 MPa (a), 500 MPa (b) and 740 MPa (c). The mapping results of Ca Kα1 is presented correspondingly. For other elements: C, O, P, S, and Zn, their mapping results are reported in Figure. S8.

According to the elemental distribution obtained for Ca Kα1, the calcium carbonate and other additives mainly localized in the dark areas observed on SEM images. A similar distribution was also found for other elements (see Figure. S8). The FIB cut is done on these dark areas. The SEM/EDS results on the a-C:H disk at 320 MPa, 500 MPa and 740 MPa toward the presence of only C and O (in Figure. S9).

The observation of the steel rings' cross-section with TEM provided insight into the structure and the thickness of the calcium carbonate-rich tribofilms. The TEM observation results at the contact pressure of

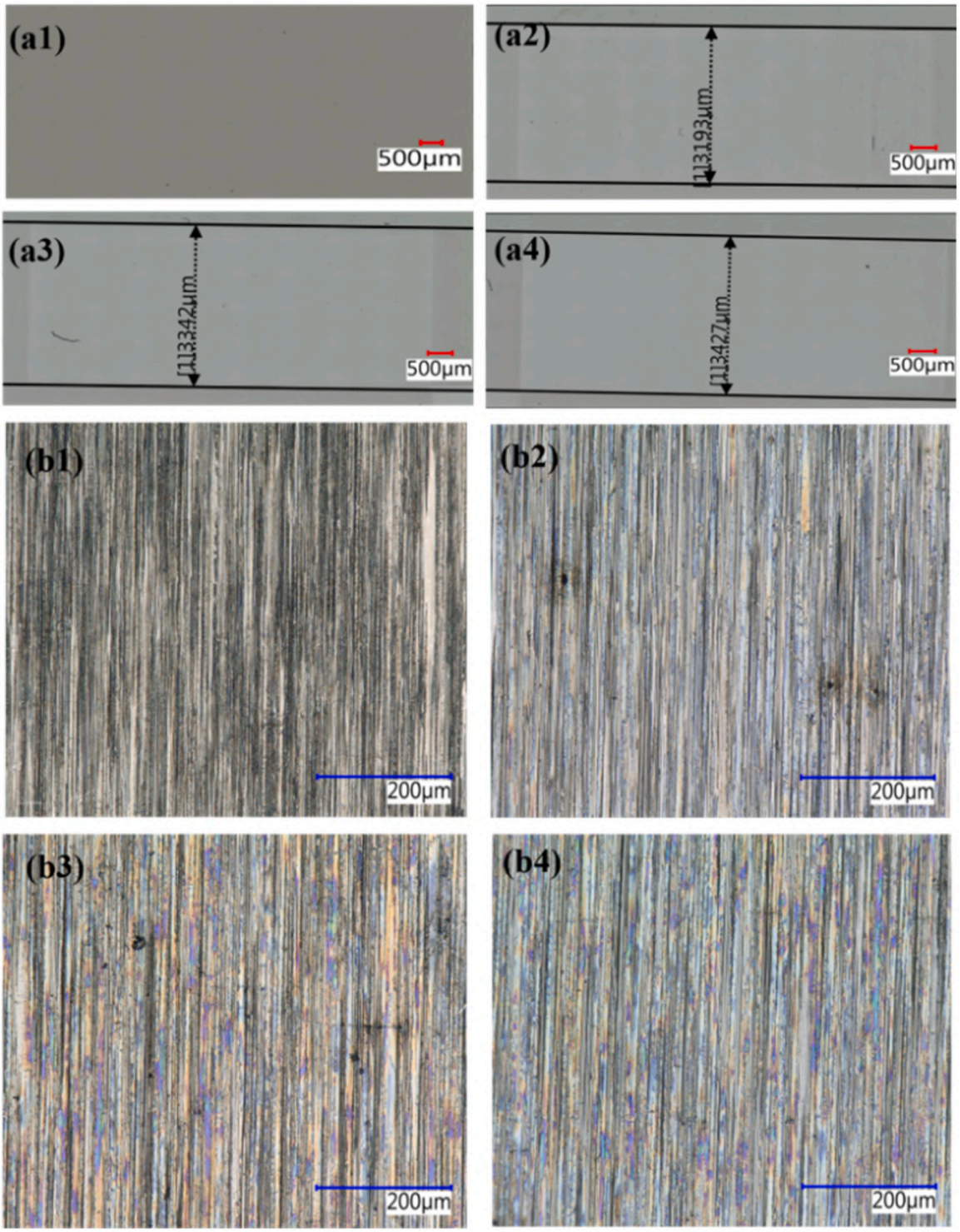

Fig. 3. Optical images of a-C:H DLC at 0 MPa (a1, no friction, i.e., reference sample), 320 MPa (a2), 500 MPa (a3) and 740 MPa (a4); optical images of steel rings at 0 MPa (b1, no friction, i.e., reference sample), 320 MPa (b2), 500 MPa (b3) and 740 MPa (b4).

320 MPa, 500 MPa and 740 MPa are given in Fig. 6(a), (b) and (c), respectively.

At 320 MPa, Fig. 6(a), the thickness of the tribofilm is in a range of 100 to 180 nm due to the fact that the tribofilm was formed on a gap. This gap can either be the groove on very rough surface or an area where a piece of iron is worn from the surface during the sliding tests. Holes and/or low weight areas (marked in red circles, Fig. 6a) are observed in the tribofilm. This could be explained by a non-homogeneous tribofilm. By comparison, the tribofilm thickness at 500 MPa (Fig. 6b) is about 110 nm. The shape between the tribofilm and the steel substrate is more homogenous than that of 320 MPa. At 740 MPa (Fig. 6c), the thickness of the tribofilm is around 120 nm. Moreover, the tribofilm itself appears more homogeneously than those of 320 MPa and 500 MPa. The shape between the steel substrate and the tribofilm is the most regular one. The difference of chemical composition on low atomic weight areas for the three steel rings was analyzed by EDS point analysis and is shown in Figure. S10.

EDS quantification was carried out from the three different

Table 2
Atomic concentrations of C, O, Fe, P, S, Ca and Zn on steel ring and a-C:H DLC disk as the function of pressure.

Elements	Atomic concentration (%)					
	Steel ring			a-C:H DLC disk		
	320 MPa	500 MPa	740 MPa	320 MPa	500 MPa	740 MPa
C	17.2	21.5	31.6	84.0	88.3	91.6
O	55.4	53.6	51.3	11.7	8.8	6.6
Fe	10.5	6.8	6.0	/	/	/
P	2.0	2.4	2.8	1.1	0.6	0.2
S	3.3	2.0	1.8	0.6	0.6	0.4
Ca	*6.9*	*9.7*	*11.1*	*2.0*	*1.3*	*0.9*
Zn	4.9	3.7	3.4	0.5	0.4	0.2

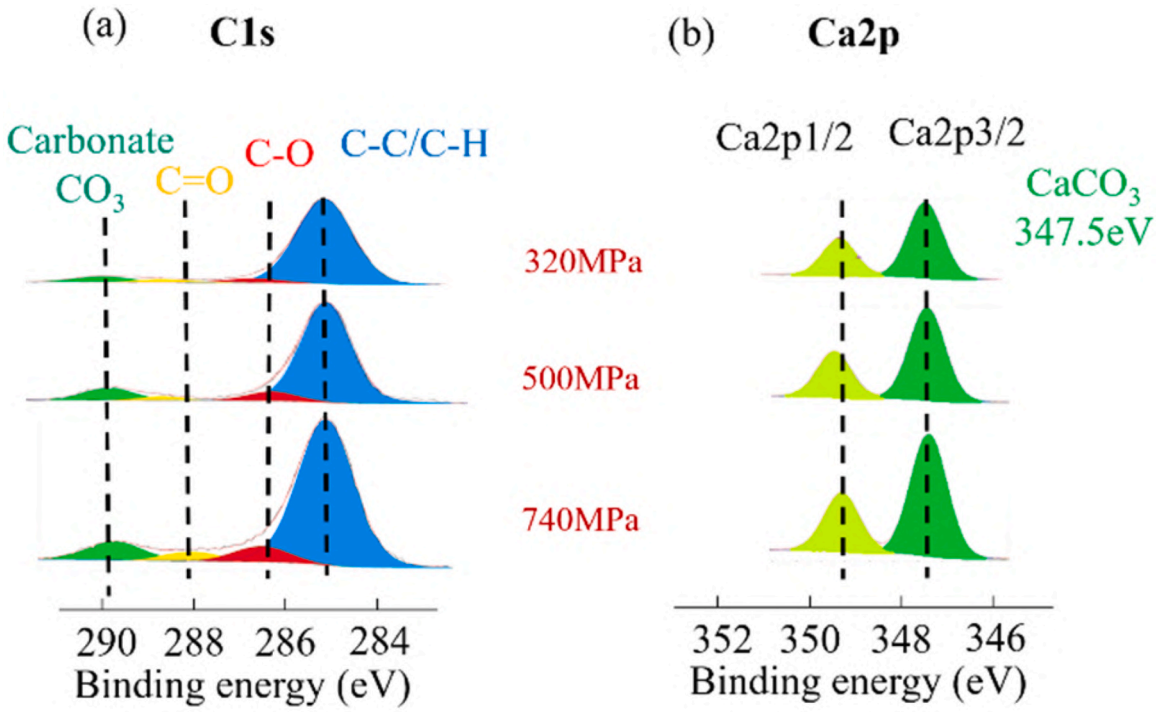

Fig. 4. Photo-peaks fitting for C1s (a) and Ca2p (b) at 320 MPa, 500 MPa and 740 MPa recorded on the steel rings (the spectra were renormalized, its height has no relation to the quantification, the original spectra are given in Fig. S7).

Table 3
Full-width-half-maximum (FWHM) and binding energies (BE) of C1s and Ca2p3/2 photo-peaks.

	320 MPa		500 MPa		740 MPa	
	Carbonate (C1s)	Ca2p3/2	Carbonate (C1s)	Ca2p3/2	Carbonate (C1s)	Ca2p3/2
BE (eV)	289.80	347.39	289.80	347.47	290.08	347.55
FWHM	1.39	1.68	1.50	1.59	1.60	1.66

tribofilms. Considering the fact that the tribofilm is not very homogeneous and especially at 320 MPa, several zones are selected (Figure. S11). The atomic ratio of Fe, Ca and (P + S+Zn)/Ca as the function of pressure is plotted in Fig. 7.7(a) and (b), respectively. It shows the evolution of the chemical composition.

In Fig. 7(a), the content of Ca and Fe exhibit the completely opposite trend with the increasing contact pressure. The increase of the Ca content is in agreement with the quantification realized by XPS. And the content reduction of Fe as the function of pressure indicates that the tribofilm (in Fig. 6a - only for the contact pressure of 320 MPa) is more possibly formed on the area where the wear occurred during the friction, rather than the groove on very rough surface. In Fig. 7(b), the ratio of (P + S+Zn)/Ca significantly decreases as the function of the contact pressure. This indicates that the tribofilm is richer in Ca when the pressure increases.

Diffraction mode was made on the cross-sections of steel rings. The crystal structures were determined by measuring the d-distance (measured by Gatan, GMS3) for each of the three pressures. The d-distance values are listed in Fig. 8.

At low and medium loads, iron disulfide and vaterite (Fig. 8a) or aragonite (Fig. 8b), two polymorphs of the calcium carbonate, are found into the tribofilm. At high load, iron disulfide is no more detected, and calcium carbonate is found in the form of calcite (Fig. 8c). To verify the calcite structure of the calcium carbonate at 740 MPa, the cross-section was also characterized by high resolution Titan TEM (Fig. 8d). The d-distance values were measured again, but more precisely thanks to the

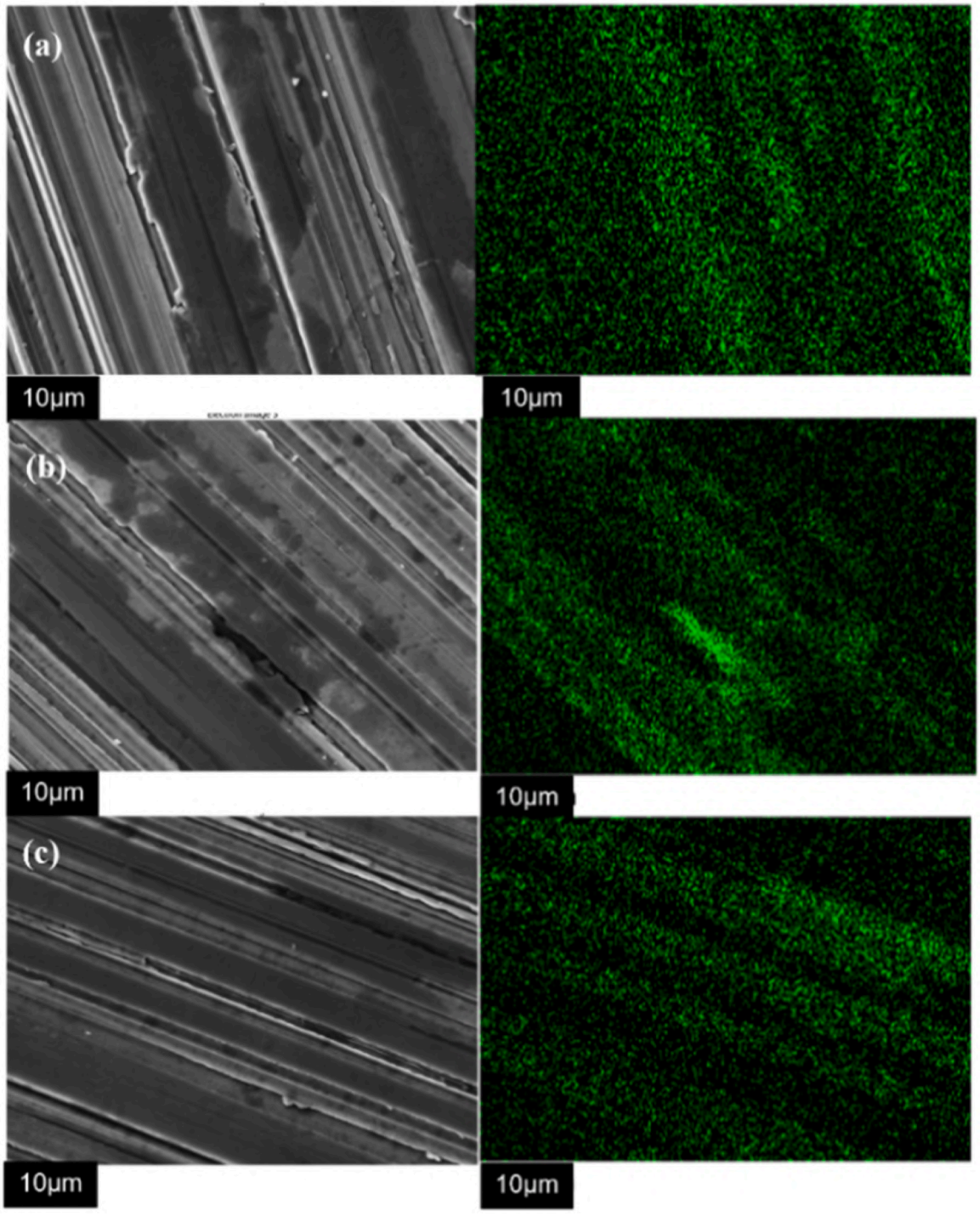

Fig. 5. SEM images on the steel rings and mapping results of Ca Kα1 obtained at 320 MPa (a), 500 MPa (b) and 740 MPa (c).

better resolution. A good match between the experimental and theoretical values of calcite was confirmed.

The presence of vaterite, aragonite, and calcite at different contact pressures was also confirmed by FTIR spectroscopy carried out in reflection mode (Fig. 9).

By comparing with the raw steel ring (before friction), the spectra recorded after friction tests display more significant peaks located at around 860 cm^{-1} and 880 cm^{-1}. The peak at 860 cm^{-1} is assigned to the aragonite, while the one at 880 cm^{-1} was attributed to vaterite and/or calcite [29–31]. By combining the FTIR and TEM results, the comprehensive characterization of the calcium carbonate phases in the tribofilm is provided. At 320 MPa, the majority of calcium carbonate was in the form of vaterite, together with a little component of aragonite. At 500 MPa, the predominant polymorph of $CaCO_3$ was aragonite, with a small amount of vaterite/calcite. Finally, at 740 MPa $CaCO_3$ underwent a transition phase from aragonite to calcite.

4.3. Detergent additive characterization by TEM

The most abundant polymorph of $CaCO_3$ in the tribofilm changed from vaterite (320 MPa), to aragonite (500 MPa) and finally to calcite (740 MPa). In order to compare with the structure of the detergent

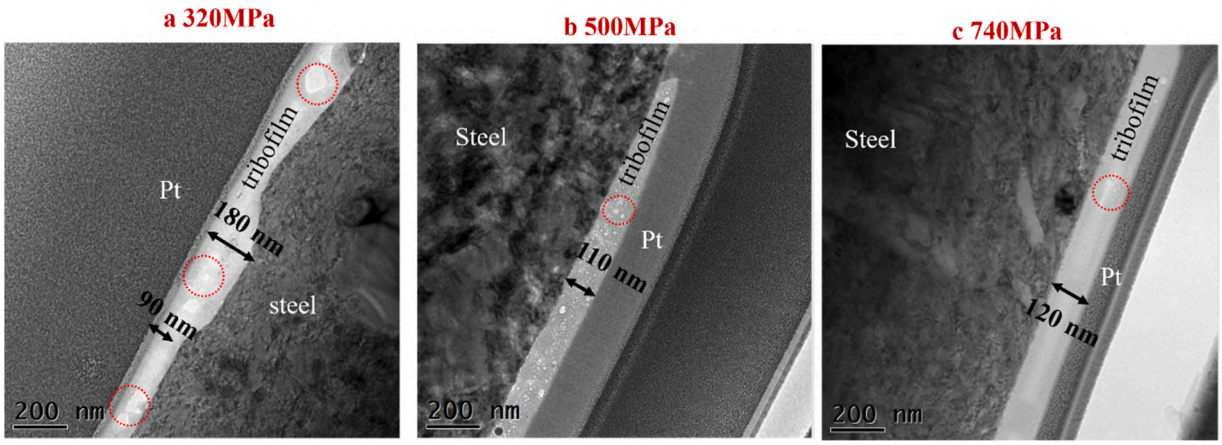

Fig. 6. TEM/FIB cross-section of steel rings at 320 MPa (a), 500 MPa (b) and 740 MPa (c).

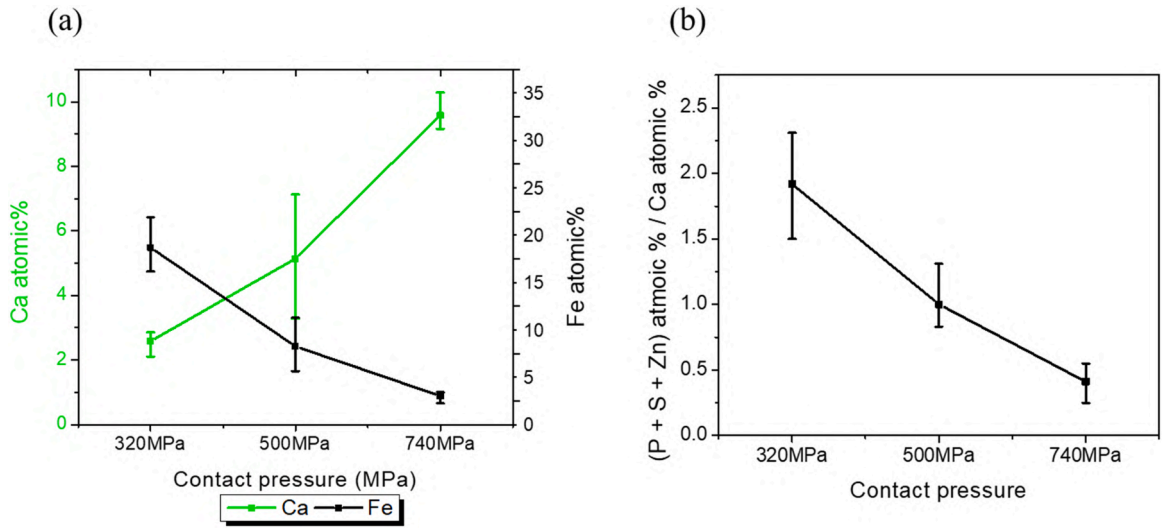

Fig. 7. The atomic ratio of Ca, Fe (a) and (P + S+Zn)/Ca (b) obtained by FIB-TEM/EDS.

present in the fully formulated oil, the detergent particles were extracted directly from the additive and were observed by TEM in diffraction mode. The extraction process is detailed in Figure. S12. The size of the particles was in the range of 200 nm to 400 nm (Fig. 10a). The EDS spectrum justified that these particles are rich in detergent components (Fig. 10b). Diffraction mode clearly indicated that the structure is amorphous (Fig. 10c). These results would therefore state that the detergent particles underwent significant structural modifications (crystallization) under tribological stress, these modifications being at the origin of the observed tribological properties. The nature of the crystallographic phase would also affect the tribological performance.

4.4. Numerical simulations

From the different experimental characterizations, it appears evident that several concurrent factors determine the tribological behavior of the oil-lubricated steel/a-C:H DLC contact. The presence of a multi-component fluid medium, possible defects such as vacancies and grain boundaries, and the amorphous structure of DLC coating play a role in the frictional processes. However, their contribution should be the same on average for all the conditions which were considered experimentally. Therefore, we expect that the CoF reduction at increased contact pressures is mainly related to the intrinsic lubricity of the calcium carbonate polymorph composing the tribofilm, as well as its improvement in homogeneity and density.

To shed light on this question we have performed DFT simulations of the intrinsic $CaCO_3$ @$CaCO_3$ interfaces and extrinsic $CaCO_3$ @diamond interfaces, for each of the three different $CaCO_3$ crystalline phases. The extensive characterizations presented in the previous chapters pointed toward the formation of a tribofilm almost over the steel disk, suggesting that the tribo-contact is occurring between the tribofilm (CaCO3-based) and the DLC coated disk, i.e, not directly involving the steel disk. The surface reactivity of hydrogenated diamond is expected to be like that of hydrogenated DLC as both dominated by dispersion interactions due to the same hydrogen termination. Therefore, our models are representative of contacts between micro- and nano-asperities that can occur under boundary lubrication and mixed lubrication regimes. We considered two types of sliding interfaces due to uncertainty about the sliding mechanism that occurs during real experiments: the $CaCO_3$ @$CaCO_3$ models are representative of a situation where the sliding interface is embedded within the tribofilm, while the $CaCO_3$ @diamond interfaces represent the opposite case, in which a hydrogen-passivated diamond surface is sliding on $CaCO_3$.

The work of separation (W_{SEP}) for the intrinsic $CaCO_3$ @$CaCO_3$ and extrinsic $CaCO_3$ @diamond interfaces is depicted in Fig. 11(a). W_{SEP} represents the energy per area required to separate two mated surfaces, and dictates the adhesive friction [32,33]. The W_{SEP} values for the intrinsic interfaces are about two orders of magnitude higher than those involving the extrinsic H-passivated diamond surface. The large difference arises from the different types of interactions that are involved. The

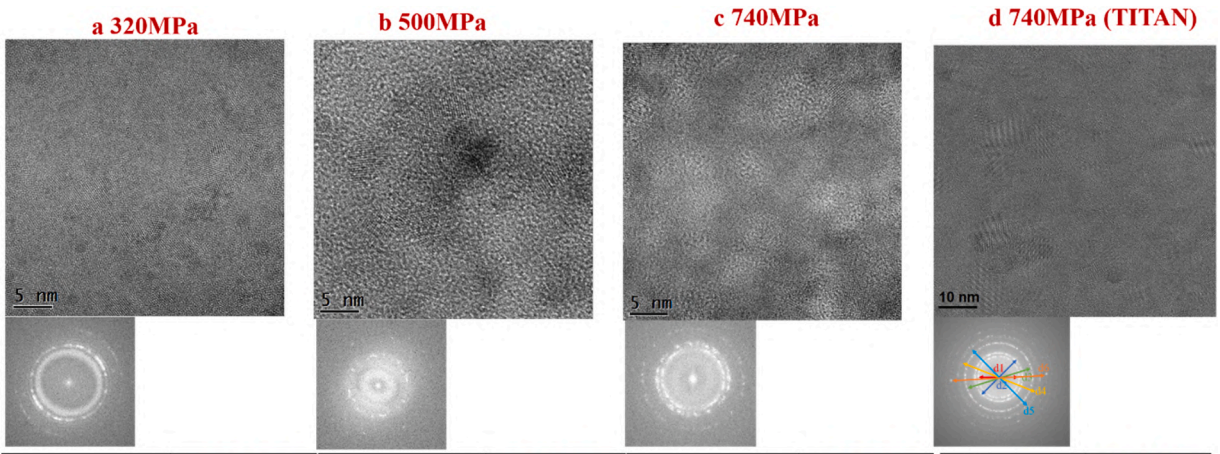

d distance (Å)	320MPa
3.11	FeS_2*
2.42	FeS_2*
2.13	Vaterite
1.75	Vaterite

d distance (Å)	500MPa
3.27	Aragonite
3.11	FeS_2*
1.90	Aragonite
1.72	Aragonite

d distance (Å)	740MPa
2.84	***Calcite***
2.49	***Calcite***
1.87	***Calcite***
1.72	*Aragonite*

d distance (Å)	740MPa
d1=2.84	**Calcite**
d2=2.49	**Calcite**
d3=1.87	**Calcite**
d4=1.56	**Calcite**
d5=1.50	**Calcite**
d6=1.33	**Calcite**

Fig. 8. TEM diffraction mode on cross-sections and d-distance measurements (tables below) at 320 MPa (a), 500 MPa (b), 740 MPa (c) and 740 MPa verified by Titan microscope(d) [26–28].

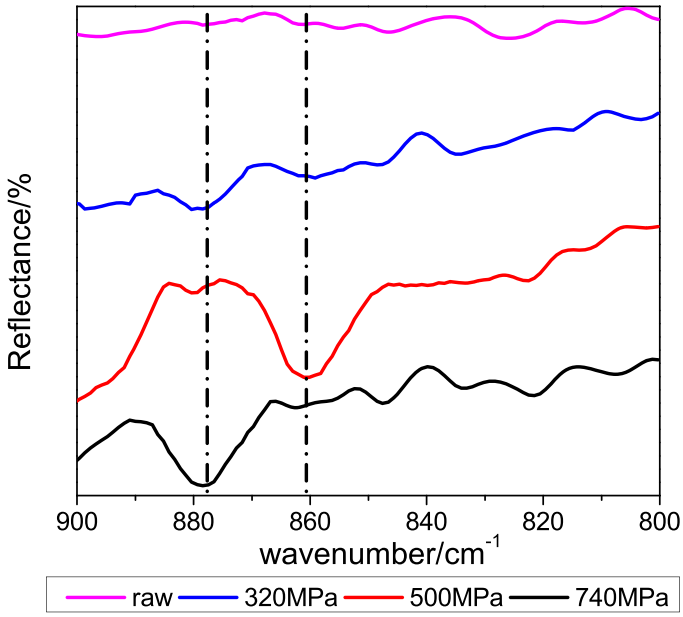

Fig. 9. FTIR characterization on virgin steel ring (pink line) and on wear tracks of steel ring at 320 MPa (blue line), 500 MPa (red line) and 740 MPa (black line).

widespread network of ionic bonds between Ca^{2+} and CO_3^{2-} makes the surfaces of calcium carbonate very sticky to each other. However, the W_{SEP} values drop close to zero when the $CaCO_3$ counter-surface is replaced by the inert diamond surface fully passivated by H atoms. Interestingly, the W_{SEP} for the homogeneous interfaces of calcite (0.009 J/m^2), aragonite (0.017 J/m^2) and vaterite (0.021 J/m^2) are ordered following the same trend observed for the experimental friction coefficients. Although the differences between the values are very small, this result points toward the possibility of a polymorph-dependent lubricity of $CaCO_3$.

In Fig. 11(b), the potential corrugation ΔW_{SEP} is depicted as a function of the applied normal load for the $CaCO_3$ @$CaCO_3$ interfaces. In this regard, ΔW_{SEP} represents the maximum energetic barrier that the mated surfaces need to overcome during mutual sliding. In previous works, we have reported the ΔW_{SEP} correlates well with the static friction coefficient of many homogeneous interfaces. Looking at the blue line in Fig. 11(b), the calcite@calcite potential corrugation is the lower regardless of the applied pressure. Showing higher ΔW_{SEP} values, vaterite@vaterite and aragonite@aragonite interfaces seems to be less slippery. The calcite polymorph turned out to be the most slippery also according to the tribological experiment.

The numerical results on the W_{SEP} property suggest that sliding processes most likely occur at the interface between the $CaCO_3$-composed tribofilm and the DLC surface. For an in-depth analysis, we carried out ab initio molecular dynamics of the $CaCO_3$ @diamond interfaces, as represented in Fig. 12.

To impose tribological conditions, AIMDs were performed at 300 K by constraining the velocity of the outmost carbon atoms to 200 m/s (= 2 A ps^{-1}) along the *x*–direction, and by applying 1 GPa of external pressure onto them, while freezing the dynamic of the basal Ca atoms of the $CaCO_3$ surface. The resistive force experienced by the dragged carbon atoms along the sliding direction was recorded along 18 *ps* of dynamic, while the shear stress is simply obtained by dividing the resistive force by the surficial area. In Fig. 12, we have plotted the cumulative average of the shear stress as a function of time for the diamond-based interfaces with calcite (blue line), vaterite (black line) and aragonite (orange line). For calcite and vaterite, the shear stress immediately converges to values much lower than 0.02 GPa. Conversely, the sliding between aragonite and diamond seems to produce higher friction forces. However, the difference in the shear stress values for the three $CaCO_3$ polymorphs sliding against diamond is very small. The shear stress as well as the differences among the polymorphs may increase by reducing the H-passivation of the diamond surface. While the study of the effects of intermediate H coverages is the subject of a forthcoming work, the limiting case of full H-coverage here considered is relevant as it

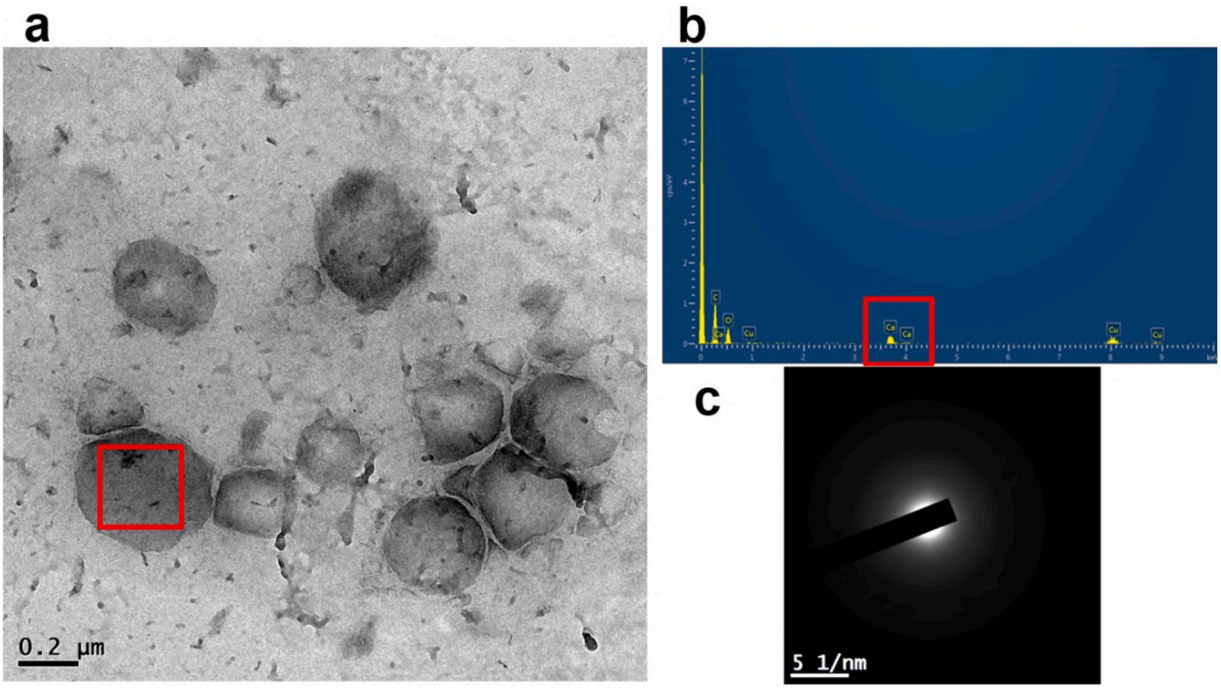

Fig. 10. TEM bright field image of detergent particles (a), the EDS pointID spectrum (b) and diffraction mode (c).

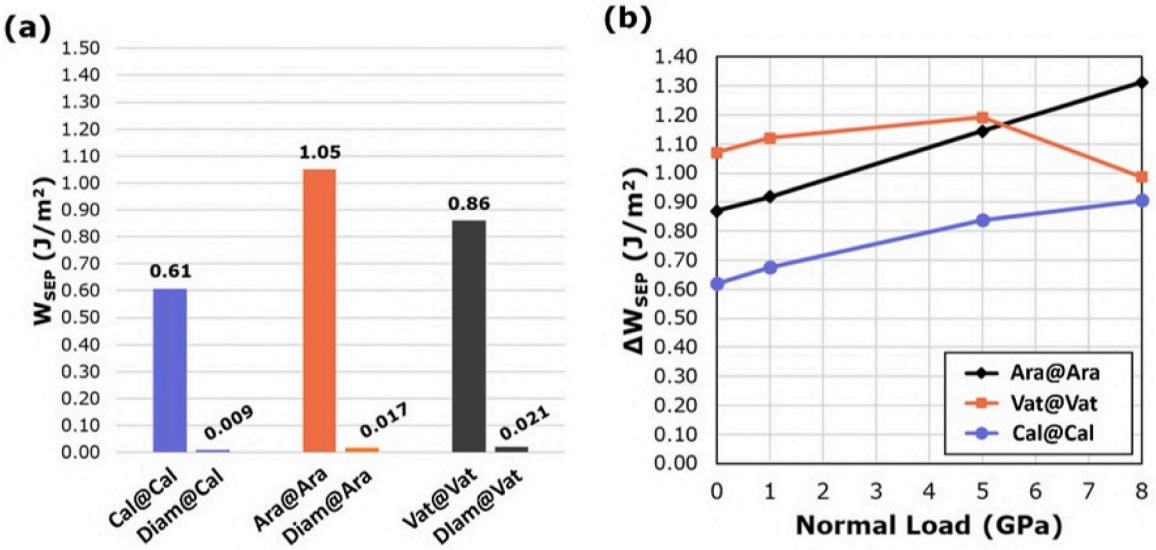

Fig. 11. Work of Separation (W_{SEP}) values for the homogeneous interfaces of calcite (Cal@Cal), aragonite (Ara@Ara), vaterite (Vat@Vat), and for the heterogeneous interfaces involving the H-passivated diamond (Diam@) surface (a). Potential energy corrugation (ΔW_{SEP}) as a function of the external load applied perpendicularly to the $CaCO_3$ @$CaCO_3$ interfaces (b).

represents the opposite case with respect to the intrinsic sliding in $CaCO_3$.

5. Discussions

In this study, the effect of the contact pressure on friction is investigated in steel/a-C:H DLC mixed contact with a fully formulated 5W30 engine oil, under boundary/mixed lubrication regime. The formation of a calcium carbonate-rich patchy tribofilm onto the steel rings was clearly characterized by SEM and XPS, while only few traces of additives elements were detected on the a-C:H DLC counterpart. The amorphous calcium carbonate in detergent additive from engine oil is justified by the TEM characterization. However, during the friction tests performed at 320 MPa, 500 MPa and 740 MPa, the amorphous calcium carbonate from the engine oil mainly crystallizes to vaterite, aragonite and calcite crystalline structures, respectively. Both the crystallization of $CaCO_3$ and its phase transitions were confirmed by TEM-FIB and FTIR.

The interaction between the calcium carbonate detergent and the ZDDP wear-resistant additive, both contained in the oil, was not investigated in this work. However, based on the results of previous researches, the anti-wear performance of ZDDP is disrupted with the presence of Ca-based detergent agents. For some early studies, the disruption was explained by the longer induction time of ZDDP induced by the overbased detergent co-additive in lubricant. In presence of overbased detergent additive, ZDDP decomposition rate is slowed down or the required decomposition temperature needs to be higher [34–40].

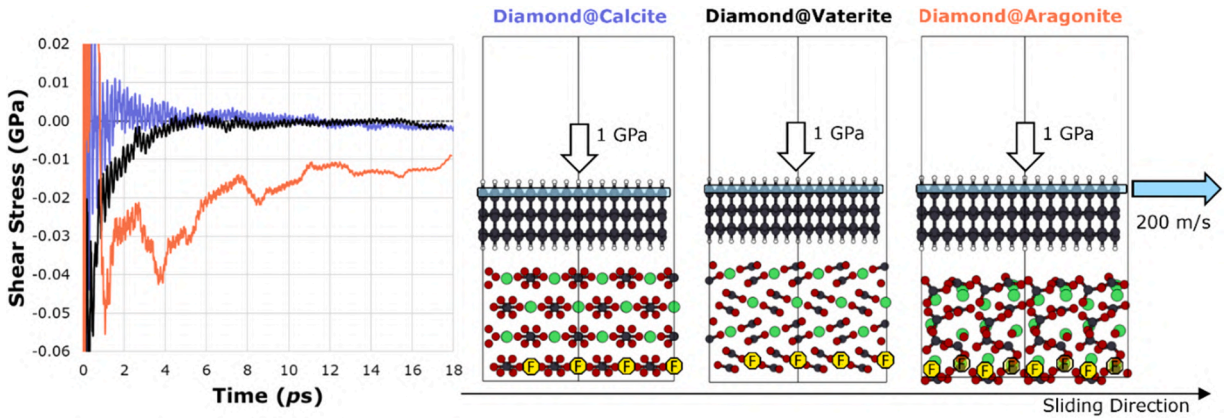

Fig. 12. the cumulative average of the shear stress as a function of time for the diamond-based interfaces with calcite (blue line), vaterite (black line) and aragonite (orange line).

Later on, some researches justified by XANES that the Ca^{2+} cation can integrate into polyphosphate chain length by replacing Zn^{2+}. The occurrence of integration was due to the fact that Ca^{2+} is a harder Lewis acid than Zn^{2+}, and phosphate was also a hard Lewis base. As the results, phosphates prefer to link with Ca^{2+} based on the Lewis acid-base theory [11,16,41,42]. A common point of all of these studies is that the concentration of ZDDP related elements is lower in presence of detergent. Furthermore, the presence of detergent additive could also lead to a higher CoF and reduce the anti-wear properties of ZDDP. By contrast, it was also suggested [43,44] that neutral sulphonates act as solubilizing agents, impeding the clustering of a safeguarding antiwear film. However, the situation of overbased detergent is complex because it can also generate protective antiwear films on their own, and the presence of ZDDP seems to enhance the efficacy of these films. Based on these studies, it seems that the combination of ZDDP and overbased detergent is not definitely a benefit to improve tribological performances.

In this work, the study on the tribological performances of only ZDDP or only overbased calcium carbonate detergent was not conducted to perform the comparison. However, less wear and lower friction are observed with a decrease of the content of ZDDP derived elements (Fig. 7). It is well-known from the literature that the ZDDP tribofilm prefers to form on iron [45]. This can partially explain the fact the ZDDP tribofilm formed on the carbon-based DLC coatings is found to be much thinner than that on steel surface [7,46,47]. And the tribofilm on a-C:H DLC disks was hardly visible in this study. Fig. 6 and Fig. 7 show that at higher pressure, the interlayer between the steel substrate and the tribofilm is more regular and that the quantity of Fe decreases. From this point of view, it appears that the surface wear protection is ensured by the well-known anti-wear property of overbased calcium detergent [48–52] by increasing the quantity of calcium carbonate and crystallization [36]. Therefore, in this study, the reactivity of ZDDP elements is weakened due to the presence of detergent additive, especially at high pressure where calcium carbonate plays his role, thus improving the tribological performances.

It was also found that the friction reduction as the function of pressure was tightly related to the calcium carbonate polymorph structure. The friction reduction effect of overbased detergent additive with amorphous or crystalline structures has been mentioned in references 36 and 53, but not much details were given. Meanwhile, some studies also reported that the amorphous/vaterite calcium carbonate core in detergent additive can crystallize into calcite during the friction. For example, the calcite was justified by Raman spectroscopy [24], Infrared Reflection Absorption Spectroscopy by Fourier transform and Polarisation Modulation (PM-IRRAS) [54], XANES and ToF-SIMS [55]. In another study, X ray techniques justified the calcite polymorph obtained by shear strains during grinding process [56]. Based on these publications, the crystallization mechanism was attributed to contact pressure and shearing. On the other hand, the polymorph structure-dependent friction behavior was only reported in reference 24, but this study used a crystalline calcium carbonate core rather than an amorphous one. Moreover, none of these researches present a direct observation of calcium carbonate polymorphs or reveal a clear relation between CoF and the polymorph structure.

In our work, we reported the crystallization of calcium carbonate from amorph to crystal under tribological solicitation. It was also demonstrated that the polymorph structure is load-dependent. These polymorph species are directly observed and characterized by TEM/FIB. However, the detailed mechanism of crystallization and crystalline transformation are extremely complex. It can be supposed that these structural changes are related to the energy dissipation induced by load and shear, considering the order of thermodynamic stability of the three polymorphic forms are: vaterite < aragonite < calcite. From our DFT analysis on the tribological properties W_{SEP} and ΔW_{SEP} of $CaCO_3$ polymorphs interfaces, calcite seems to possess the most valuable inherent lubricity.

6. Conclusions

This study investigated the mechanism of friction reduction as the function of pressure in boundary/mixed lubrication regime, for steel/a-C:H DLC mixed tribo-pair lubricated with a commercial fully formulated 5W30 engine oil. By coupling multiple surface analysis techniques, the increase of quantity of calcium carbonate with the contact pressure, which was originated from detergent additive, was confirmed. The calcium carbonate not only acts as give anti-wear agent but also to reduce the friction by different polymorphs of crystal. The main polymorph of calcium carbonate in the tribofilm at low contact load was vaterite, then transforming to aragonite and calcite as the contact load increases.

The DFT simulation indicate that the calcite provides the best lubricity among the three polymorphs. More importantly, the experimental results are partially justified by the W_{sep} values of H-passivated diamond@$CaCO_3$ interfaces. Therefore, one of the strategies to control the friction would be realized by load-induced $CaCO_3$ polymorphs modification.

Future works

The authors intend to perform the friction tests at different contact loads with the corresponding base oil of this fully formulated 5w30 engine oil plus overbased detergent to investigate the tribological behaviors. Meanwhile, the conventional ball-on-disk friction tests in more severe conditions are expected, this is to most probably avoid the effect of fluid properties in mixed lubrication regime. Besides, the impact of

contact pressure with different structures of overbased detergent additive should be investigated to highlight the role of calcium carbonate polymorphs in friction reduction. At last, the numerical simulation will be conducted to reveal the friction reduction and crystal transformation of calcium carbonate allotropes.

Statement of originality

2) The paper has not been published previously, that it is not under consideration for publication elsewhere, and that if accepted it will not be published elsewhere in the same form, in English or in any other language, without the written consent of the publisher.
3) The paper does not contain material which has been published previously, by the current authors or by others, of which the source is not explicitly cited in the paper.

Author contributions

The manuscript was written through contributions of all authors. All authors have given approval to the final version of the manuscript. These authors contributed equally: ‡E. Marquis and ‡M. Clelia Righi, §J. Galipaud and § F. Dubreuil, †E. Macron and †J. Dufils, ※F. Dassenoy and ※M. I. De Barros Bouchet.

Declaration of Competing Interest

The authors declare the following financial interests/personal relationships which may be considered as potential competing interests: Maria-Isabel De Barros Bouchet reports financial support was provided by Central College Lyon. Maria Clelia Righi reports financial support was provided by University of Bologna Department of Physics and Astronomy 'Augusto Righi'. If there are other authors, they declare that they have no known competing financial interests or personal relationships that could have appeared to influence the work reported in this paper.

Data Availability

Data will be made available on request.

Acknowledgements

The authors acknowledge the European Union and the Auvergne-Rhône-Alpes region for the funding of FEDER project, PLATEFORME TRIBLOGIE MOTEURS. The authors also appreciate the "Advancing Solid Interface and Lubricants by First Principles Material Design (SLIDE)" project funded by the European Research Council (ERC) under the European Union's Horizon 2020 research and innovation program (Grant Agreement No. 865633).

Appendix A. Supporting information

Supplementary data associated with this article can be found in the online version at doi:10.1016/j.triboint.2024.109307.

References

[1] Erdemir A, Martin JM. Superior wear resistance of diamond and DLC coatings. Curr Opin Solid State Mater Sci 2018;22(6):243–54. https://doi.org/10.1016/j.cossms.2018.11.003.
[2] Kano M, Martin JM, Yoshida K, De Barros Bouchet MI. Super-low friction of ta-C coating in presence of oleic acid. Friction 2014;2(2):156–63. https://doi.org/10.1007/s40544-014-0047-1.
[3] De Barros Bouchet MI, Martin JM, Avila J, Kano M, Yoshida K, Tsuruda T, et al. Diamond-like carbon coating under oleic acid lubrication: evidence for graphene oxide formation in superlow friction. Sci Rep 2017;7(1). https://doi.org/10.1038/srep46394.
[4] Long Y, Bouchet M-ID, Lubrecht T, Onodera T, Martin JM. Superlubricity of glycerol by self-sustained chemical polishing. Sci Rep 2019;9(1). https://doi.org/10.1038/s41598-019-42730-9.
[5] De Barros'Bouchet M, Martin J, Le-Mogne T, Vacher B. Boundary lubrication mechanisms of carbon coatings by MoDTC and ZDDP additives. Tribology Int 2005;38(3):257–64. https://doi.org/10.1016/j.triboint.2004.08.009.
[6] Vengudusamy B, Green JH, Lamb GD, Spikes HA. Tribological properties of Tribofilms formed from ZDDP in DLC/DLC and DLC/steel contacts. Tribology Int 2011;44(2):165–74. https://doi.org/10.1016/j.triboint.2010.10.023.
[7] Čoga L, Akbari S, Kovač J, Kalin M. Differences in nano-topography and tribochemistry of ZDDP tribofilms from variations in contact configuration with steel and DLC surfaces. Friction 2021;10(2):296–315. https://doi.org/10.1007/s40544-021-0491-7.
[8] Tamura Y, Zhao H, Wang C, Morina A, Neville A. Interaction of DLC and B4C coatings with fully formulated oils in boundary lubrication conditions. Tribology Int 2016;93:666–80. https://doi.org/10.1016/j.triboint.2015.02.029.
[9] Kosarieh S, Morina A, Lainé E, Flemming J, Neville A. Tribological performance and tribochemical processes in a DLC/steel system when lubricated in a fully formulated oil and base oil. Surf Coat Technol 2013;217:1–12. https://doi.org/10.1016/j.surfcoat.2012.11.065.
[10] O'Connor SP, Crawford J, Cane C. Overbased lubricant detergents – a comparative study. Lubr Sci 1994;6(4):297–325. https://doi.org/10.1002/ls.3010060402.
[11] Wan Y, Kasrai M, Bancroft GM, Zhang J. Characterization of tribofilms derived from zinc dialkyldithiophosphate and salicylate detergents by X-ray absorbance near edge structure spectroscopy. Tribology Int 2010;43(1–2):283–8. https://doi.org/10.1016/j.triboint.2009.06.005.
[12] Costello MT, Kasrai M. Study of surface films of overbased sulfonates and sulfurized olefins by X-ray absorption near edge structure (XANES) spectroscopy. Tribology Lett 2006;24(2):163–9. https://doi.org/10.1007/s11249-006-9155-z.
[13] Topolovec-Miklozic K, Forbus TR, Spikes H. Film forming and friction properties of overbased calcium sulphonate detergents. Tribology Lett 2007;29(1):33–44. https://doi.org/10.1007/s11249-007-9279-9.
[14] Nassar AM, Ahmed NS, Abdel-Hameed HS, El-Kafrawy AF. Synthesis and utilization of non-metallic detergent/dispersant and antioxidant additives for lubricating engine oil. Tribology Int 2016;93:297–305. https://doi.org/10.1016/j.triboint.2015.08.033.
[15] Ahmed NS, Nassar AM, Abdel-Hameed HS, El-Kafrawy AF. Preparation, characterization, and evaluation of some Ashless detergent/dispersant additives for lubricating engine oil. Appl Petrochem Res 2015;6(1):49–58. https://doi.org/10.1007/s13203-015-0110-5.
[16] Reyes M, Neville A. The effect of anti-wear additives, detergents and friction modifiers in boundary lubrication of traditional Fe-base materials. Tribology Ser 2003:57–65. https://doi.org/10.1016/s0167-8922(03)80119-0.
[17] Ahmed NS, Nassar AM, Abdel-Azim A-AA. Synthesis and evaluation of some detergent/dispersant Additives for lube oil. Int J Polym Mater 2007;57(2):114–24. https://doi.org/10.1080/00914030701392385.
[18] Salinas Ruiz VR, Kuwahara T, Galipaud J, Masenelli-Varlot K, Hassine MB, Héau C, et al. Interplay of mechanics and chemistry governs wear of diamond-like carbon coatings interacting with ZDDP-additivated lubricants. Nat Commun 2021;12(1). https://doi.org/10.1038/s41467-021-24766-6.
[19] Dowson, D. (1970). Elastohydrodynamic lubrication. NASA, WASHINGTON INTERDISCIPLINARY APPROACH TO THE LUBRICATION OF CONCENTRATED CONTACTS 1970.
[20] Dowson D. Elastohydrodynamic and micro-elastohydrodynamic lubrication. Wear 1995;190(2):125–38. https://doi.org/10.1016/0043-1648(95)06660-8.
[21] Giannozzi P, Baroni S, Bonini N, Calandra M, Car R, Cavazzoni C, et al. Quantum espresso: A modular and open-source software project for quantum simulations of materials. J Phys: Condens Matter 2009;21(39):395502. https://doi.org/10.1088/0953-8984/21/39/395502.
[22] Perdew JP, Burke K, Ernzerhof M. Generalized gradient approximation made simple. Phys Rev Lett 1996;77(18):3865–8. https://doi.org/10.1103/physrevlett.77.3865.
[23] Zhang M, Li J, Zhao J, Cui Y, Luo X. Comparison of CH4 and CO_2 adsorptions onto Calcite (10.4), Aragonite (011) Ca, and Vaterite (010) CO3 surfaces: an MD and DFT investigation. ACS Omega 2020;5(20):11369–77. https://doi.org/10.1021/acsomega.0c00345.
[24] De Leeuw NH, Parker SC. Surface structure and morphology of calcium carbonate polymorphs calcite, aragonite, and Vaterite: an atomistic approach. J Phys Chem B 1998;102(16):2914–22. https://doi.org/10.1021/jp973210f.
[25] Kajita S, Pacini A, Losi G, Kikkawa N, Righi MC. Accurate Multiscale simulation of frictional interfaces by quantum mechanics/Green's function molecular dynamics. J Chem Theory Comput 2023;19(15):5176–88. https://doi.org/10.1021/acs.jctc.3c00295.
[26] Ye Y, Smyth JR, Boni P. Crystal structure and thermal expansion of aragonite-group carbonates by single-crystal X-ray diffraction. Am Mineral 2012;97(4):707–12. https://doi.org/10.2138/am.2012.3923.
[27] Donald LG. Crystallographic tables for the rhombohedral carbonates. Am Mineralogist 1961;46:1283–316 (November-December).
[28] Gomes A, Mendonça MH, da Silva Pereira MI, Costa FMA. Iron sulfide electrodeposits: effect of heat treatment on composition and structure. J Solid State Electrochem 2000;4(3):168–76. https://doi.org/10.1007/s100080050015.
[29] Liu D, Zhao G, Wang X. Tribological performance of lubricating greases based on calcium carbonate polymorphs under the boundary lubrication condition. Tribology Lett 2012;47(2):183–94. https://doi.org/10.1007/s11249-012-9976-x.

[30] Chakrabarty D, Mahapatra S. Aragonite crystals with unconventional morphologies. J Mater Chem 1999;9(11):2953–7. https://doi.org/10.1039/a905407c.
[31] Ni M. Nacre surface transformation to hydroxyapatite in a phosphate buffer solution. Biomaterials 2003;24(23):4323–31. https://doi.org/10.1016/s0142-9612(03)00236-9.
[32] Wolloch M, Levita G, Restuccia P, Righi MC. Interfacial charge density and its connection to adhesion and frictional forces. Phys Rev Lett 2018;121(2). https://doi.org/10.1103/physrevlett.121.026804.
[33] Wolloch M, Losi G, Ferrario M, Righi MC. High-throughput screening of the static friction and ideal cleavage strength of solid interfaces. Sci Rep 2019;9(1). https://doi.org/10.1038/s41598-019-49907-2.
[34] Willermet PA, Dailey DP, Carter RO, Schmitz PJ, Zhu W, Bell JC, et al. The composition of lubricant-derived surface layers formed in a lubricated cam/tappet contact II. Effects of adding overbased detergent and dispersant to a simple ZDTP solution. Tribology Int 1995;28(3):163–75. https://doi.org/10.1016/0301-679x(95)98964-f.
[35] Shirahama S, Hirata M. The effects of engine oil additives on Valve Train Wear. Lubr Sci 1989;1(4):365–84. https://doi.org/10.1002/ls.3010010405.
[36] Rounds FG. Additive interactions and their effect on the performance of a zinc dialkyl dithiophosphate. A S L E Trans 1978;21(2):91–101. https://doi.org/10.1080/05698197808982864.
[37] Yamaguchi ES, Ryason PR, Yeh SW, Hansen TP. Boundary Film Formation by ZnDTPs and detergents using ECR. Tribology Trans 1998;41(2):262–72. https://doi.org/10.1080/10402009808983747.
[38] Spikes HA. Additive-additive and additive-surface interactions in lubrication. Lubr Sci 1989;2(1):3–23. https://doi.org/10.1002/ls.3010020102.
[39] Kasrai M, Vasiga M, Suominen Fuller M, Bancroft GM, Fyfe K. Study of the effects of ca sulfonate on antiwear film formation by X-ray absorption spectroscopy using synchrotron radiation. J Synchrotron Radiat 1999;6(3):719–21. https://doi.org/10.1107/s0909049598016574.
[40] Smith GC. Surface analytical science and automotive lubrication. J Phys D: Appl Phys 2000;33(20). https://doi.org/10.1088/0022-3727/33/20/201.
[41] Wan Y, Suominen Fuller ML, Kasrai M, Bancroft GM, Fyfe K, Torkelson JR, et al. Effects of detergent on the chemistry of Tribofilms from ZDDP: studied by X-ray absorption spectroscopy and XPS. Bound Mixed Lubr – Sci Appl, Proc 28th Leeds-Lyon Symp Tribology 2002:155–66. https://doi.org/10.1016/s0167-8922(02)80017-7.
[42] Costello MT, Urrego RA. Study of surface films of the ZDDP and the MODTC with crystalline and amorphous overbased calcium sulfonates by XPS. Tribology Trans 2007;50(2):217–26. https://doi.org/10.1080/10402000701271051.
[43] Zakar, A., & Vamos, E. (1986). 'Application Testing of the Additives and Additive Packages of Ready to Start Corrosion Preventative Motor and Transmission Oils', Prcc. 5th Int. Colloq. Esslingen. 'Additives for Lubricants and Operational Fluids'.
[44] Kapsa Ph, Martin JM, Blanc C, Georges JM. Antiwear mechanism of ZDDP in the presence of calcium sulfonate detergent. J Lubr Technol 1981;103(4):486–94. https://doi.org/10.1115/1.3251714.
[45] Spikes H. The history and mechanisms of ZDDP. Tribology Lett 2004;17(3):469–89. https://doi.org/10.1023/b:tril.0000044495.26882.b5.
[46] Vengudusamy B, Green JH, Lamb GD, Spikes HA. Durability of ZDDP tribofilms formed in DLC/DLC contacts. Tribology Lett 2013;51(3):469–78. https://doi.org/10.1007/s11249-013-0185-z.
[47] Equey S, Roos S, Mueller U, Hauert R, Spencer ND, &amp, et al. Reactions of zinc-free anti-wear additives in DLC/DLC and Steel/steel contacts. Tribology Int 2008;41(11):1090–6. https://doi.org/10.1016/j.triboint.2008.03.004.
[48] Najman M, Kasrai M, Michael Bancroft G, Davidson R. Combination of ashless antiwear additives with metallic detergents: Interactions with neutral and overbased calcium sulfonates. Tribology Int 2006;39(4):342–55. https://doi.org/10.1016/j.triboint.2005.02.014.
[49] Yin Z, Kasrai M, Bancroft GM, Fyfe K, Colaianni ML, Tan KH. Application of soft X-ray absorption spectroscopy in chemical characterization of antiwear films generated by ZDDP Part II: the effect of detergents and dispersants. Wear 1997;202(2):192–201. https://doi.org/10.1016/s0043-1648(96)07273-0.
[50] Morizur MF, Teysset O. Antiwear actions of additives in solid dispersion. Lubr Sci 1992;4(4):277–99. https://doi.org/10.1002/ls.3010040405.
[51] Hong H, Riga AT, Cahoon JM. Evaluation of overbased sulfonates as extreme pressure additives in metalworking fluids. II: lithium and potassium overbased sulfonates. Lubr Eng 1993;51:147–50.
[52] Mansot JL, Hallouis M, Martin JM. Colloidal antiwear additives 2. Tribological behaviour of colloidal additives in mild wear regime. Colloids Surf A: Physicochem Eng Asp 1993;75:25–31. https://doi.org/10.1016/0927-7757(93)80412-8.
[53] Cao C, Liu G, Zhang R, She H, Tao Q. Frictional characteristics of crystalline calcium sulfonate detergent in engine oil by mini-traction machine. SAE Tech Pap Ser 2014. https://doi.org/10.4271/2014-01-2789.
[54] Cizaire L, Martin JM, Gresser E, Dinh NT, &amp, Heau C. Tribochemistry of overbased calcium detergents studied by Tof-Sims and other surface analyses. Tribology Lett 2004;17(4):715–21. https://doi.org/10.1007/s11249-004-8078-9.
[55] Palermo T, Giasson S, Buffeteau T, Desbat B, Turlet JM. Study of deposit and friction films of overbased calcium sulphonate by PM-IRRAS spectroscopy. Lubr Sci 1996;8(2):119–27. https://doi.org/10.1002/ls.3010080203.
[56] Northwood DO, Lewis D. Transformation of vaterite to calcite during grinding. Am Mineralogist 1968;53:2089–92 (November-December).